

# Simulation of Dipole Vorticity Dynamics Colliding Viscous Boundary Layer at High Reynolds Numbers

E. Ezzatneshan

*Aerospace Engineering Group, New Technologies Engineering Department, Shahid Beheshti University, Tehran, Iran*

†Corresponding Author Email: [e\\_ezzatneshan@sbu.ac.ir](mailto:e_ezzatneshan@sbu.ac.ir)

(Received July 2, 2018; accepted October 24, 2018)

## ABSTRACT

The vorticity dynamics of a Lamb-like dipole colliding with flat boundaries are investigated for high Reynolds number flows by implementation of the lattice Boltzmann method (LBM). The standard LBM based on the single-relaxation-time collision model suffers from numerical instabilities at high Reynolds numbers. Herein, a regularized collision model is employed for the LBM to preserve the stability and accuracy of the numerical solutions at such flow conditions. The computations are performed for the normal collision of the dipole with the no-slip boundary for several Reynolds numbers in the range of  $Re = 10^4 - 10^5$ . The results obtained based on the regularized lattice Boltzmann (RLB) method for the statistical flow characteristics like the vorticity field and enstrophy quantity of the dipole-wall collision problem are investigated. The present study demonstrates that the shear-layer instabilities near the wall are responsible for rolling-up of the boundary layer before it is detached from the surface for high Reynolds numbers. This detachment mechanism leads to a viscous rebound and formation of small scale vortices. The shear-layer vortices formed dramatically influence the flow evolution after the collision and result strong enhancement of the total enstrophy of the flow field. By comparing the present results with those of provided by other numerical solutions, it is also concluded that the RLB scheme implemented is robust and sufficiently accurate numerical technique in comparison with the flow solvers based on the Navier-Stokes equations for predicting the statistical features of separated fluid flows even at high Reynolds numbers.

**Keywords:** Lattice boltzmann method; Regularized collision model; Dipole vorticity dynamics; High Reynolds numbers.

## NOMENCLATURE

$c$	lattice speed	$\Delta x$	grid space
$\mathbb{C}$	collision operator	$\Omega$	vorticity
$e$	microscopic velocity vector	$\Pi$	momentum flux
$f$	distribution function	$\alpha$	discrete directions
$t$	time	$\rho$	density
$\Delta t$	time step	$\nu$	viscosity
$u$	velocity vector	$\tau$	relaxation time
$x$	coordinate vector	$\omega$	weight factor

## 1. INTRODUCTION

The interaction between the vorticity structures and no-slip surfaces in fluid turbulence is known to have a crucial importance on the evolution of flow in nature and a wide range of practical interests. For instance, the whether dispersion into a turbulent atmosphere can be influenced by large-scale

vortices colliding with coastal or mountain ridges. Also, in the aerospace engineering, the downwash vortices from aircraft wing or helicopter rotor blade interact with the ground in the takeoff and landing phases of flight which affect the air flow characteristics. Due to the appreciable effects of the vorticity dynamics in collision with the wall on the flow structures, studying of this phenomenon has

been considered by using the experimental observations (Wells and Afanasyev, 2004, Wells *et al.* 2007).

To gain in-depth insight into the physics of such flow problem in fluid mechanics, numerical approaches are efficient tool because of the rapid increase in computing capabilities in the present era and improvements made for the computational schemes developed in terms of accuracy and robustness. The early numerical studied of the dipole vorticity dynamics colliding with a no-slip wall yield many important results on the flow structures and statistics (Orlandi 1990, Coutsias and Lynov, 1991, Clercx and Heijst, 2002, Clercx and Bruneau, 2006). These reported computations have been performed by flow solvers based on the Navier-Stokes (N-S) equations and the simulations are limited to Reynolds number 5000. It is obvious that the unsteadiness and turbulence effects at higher Reynolds numbers have significant influence on the flow patterns of this problem which is not clearly addressed. There are very few numerical works based on the N-S equations for simulation of dipole-wall collision problem at high Reynolds numbers. This deficiency could be because of stability restrictions or accuracy concerns of the numerical approaches applied for simulation of the flow characteristics at high Reynolds numbers. At such flow conditions, the chaotic and unpredictable motion of fluid flow with a wide range of time and length scales ensue a complex flowfield which needs more accurate techniques for computational studies. Kramer *et al.* (2007) have employed an accurate discretization scheme for the N-S equations to study this flow problem at Reynolds numbers up to  $2 \times 10^4$ .

Recently, the lattice Boltzmann method (LBM) has become one of the most powerful alternative computational techniques to the traditional flow solvers based on the N-S equations. The LBM is widely used for numerical simulations of fluid flow problems with complex physics due to its promising advantages, like the simplicity of programming and its consistency for massively parallel computing. This method is developed based on the kinetic theory and predicts the fluid dynamics by modeling the particle interactions at the mesoscopic scale. Accordingly, ease of considering microscopic interactions for modeling of additional physical phenomenon is the other advantage of the LBM. However, the standard form of the LBM based on the single-relaxation-time (SRT) collision model suffers from inherent instability at high Reynolds number flows, which greatly restricts its application to solve engineering practical problems. This stability problem is due to the presence of a very thin boundary layer at high Reynolds number flows and the LBM solution becomes strongly anisotropic to resolve such thin layers. Thus, in order to solve high Reynolds number flows with a sufficient accuracy, a large number of uniform lattices may be used, which requires larger computer resources. Another outstanding effort to overcome this shortcoming of the standard LBM is to implement more robust and efficient collision models. The

entropic lattice Boltzmann (ELB) (Karlin *et al.* 1998), multiple-relaxation-time (MRT) (Du *et al.* 2006) and the regularized lattice Boltzmann (RLB) (Latt and Chopard 2006) methods are the most popular of the collision operators which have excellent stability characteristics for simulation of fluid flows at high Reynolds numbers. The efficiency and accuracy of these collision models have been studied in several works in the literature (Luo *et al.* 2011, Ezzatneshan 2018).

Lagrava *et al.* (2012) have applied the LBM for simulation of the dipole vorticity dynamics up to moderate Reynolds number 5000. They have used a multi-block LBM to apply a fine resolution of grid points near the wall for preserving the stability of LBM. To the best of author's knowledge, there is no another work in literature on the simulation of this flow problem by using the LBM at high Reynolds numbers. In the present work, the regularized collision model is implemented for the LBM to preserve the stability and accuracy of the numerical solution of the dipole-wall collision at high Reynolds numbers. A clear insight in the flow statistics of this problem is giving with concentrating on the vorticity dynamics close the no-slip wall. The capability and robustness of the implemented RLB scheme are also demonstrated for simulation of the active role of the dipole vorticity dynamics in the formation of detached boundary layer from the no-slip wall for a wide range of Reynolds numbers in comparison with the previous studies based on the N-S flow solvers.

The paper is structured as follows: The governing equation of the RLB scheme is presented in Section 2. Section 3 deals with discussions about the numerical results obtained for the dipole-wall collision considered. Finally, some conclusions are made in Section 4.

## 2. GOVERNING EQUATIONS

The governing generalized lattice Boltzmann equation reads:

$$f_\alpha(\mathbf{x} + \mathbf{e}_\alpha \Delta t, t + \Delta t) - f_\alpha(\mathbf{x}, t) = \mathbb{C}(f_\alpha) \quad (1)$$

where  $\alpha$  defines the discrete directions,  $f_\alpha$  is the particle (mass) distribution function,  $t$  is the time,  $\Delta t$  is the time step and  $\mathbf{e}_\alpha$  denotes the microscopic velocity of particles along the  $\alpha$ -th direction. The operator  $\mathbb{C}(f_\alpha)$  defines the change in  $f_\alpha$  due to collisions. The collision operator  $\mathbb{C}(f_\alpha)$  in the standard form of the LBM is based on the SRT which is expressed as

$$\mathbb{C}(f_\alpha) = -\frac{1}{\tau} [f_\alpha(\mathbf{x}, t) - f_\alpha^{eq}(\mathbf{x}, t)] \quad (2)$$

where  $\tau$  is the non-dimensional relaxation time parameter.  $f_\alpha^{eq}$  defines the equilibrium distribution function through a Chapman-Enskog expansion procedure which can be written as

$$f_{\alpha}^{eq} = \rho \omega_{\alpha} \left( 1 + 3 \frac{\mathbf{e}_{\alpha} \cdot \mathbf{u}}{c^2} + \frac{9}{2} \frac{(\mathbf{e}_{\alpha} \cdot \mathbf{u})^2}{c^4} - \frac{3}{2} \frac{|\mathbf{u}|^2}{c^2} \right) \quad (3)$$

In Eq. (3),  $\omega_{\alpha}$  is a weight coefficient and  $\mathbf{u} = (u, v)$  and  $\rho$  are the macroscopic velocity vector and density, respectively. For a two-dimensional (2-D) square lattice model with nine particle velocity directions (D2Q9), the discrete particle velocity  $\mathbf{e}_{\alpha}$  and the weight factors  $\omega_{\alpha}$  are given as

$$\mathbf{e}_{\alpha} = c \begin{bmatrix} 0 & 1 & 0 & -1 & 0 & 1 & -1 & -1 & 1 \\ 0 & 0 & 1 & 0 & -1 & 1 & 1 & -1 & -1 \end{bmatrix} \quad (4)$$

$$\omega_{\alpha} = \begin{cases} \frac{4}{9} & \alpha = 0 \\ \frac{1}{9} & \alpha = 1, 2, 3, 4 \\ \frac{1}{36} & \alpha = 5, 6, 7, 8 \end{cases} \quad (5)$$

where  $c = \Delta x / \Delta t$  is the lattice speed and  $\Delta x$  is the grid spacing which are assumed to be unity. The macroscopic density  $\rho$  and velocity  $\mathbf{u}$  are explicitly defined based on the particle distribution function as

$$\rho = \sum_{\alpha} f_{\alpha}, \quad \rho \mathbf{u} = \sum_{\alpha} \mathbf{e}_{\alpha} f_{\alpha} \quad (6)$$

The kinematic viscosity  $\nu$  depends on the speed of sound  $c_s = c / \sqrt{3}$  and continuous Bhatnagar–Gross–Krook (BGK) relaxation time  $\tau$  by the following definition

$$\nu = c_s^2 (\tau - 0.5) \quad (7)$$

The lattice Boltzmann equation given in Eq. (1) is solved by a streaming-collision procedure in two steps. First, the particles collide on the lattice nodes, known as ‘collision step’

$$\bar{f}_{\alpha}(\mathbf{x}, t) = f_{\alpha}(\mathbf{x}, t) - \frac{1}{\tau} [f_{\alpha}(\mathbf{x}, t) - f_{\alpha}^{eq}(\mathbf{x}, t)] \quad (8)$$

Second, propagation of the force-free particle distributions occurs according to their respective speed, known as ‘streaming step’

$$f_{\alpha}(\mathbf{x} + \mathbf{e}_{\alpha} \Delta t, t + \Delta t) = \bar{f}_{\alpha}(\mathbf{x}, t) \quad (9)$$

where  $f_{\alpha}(\mathbf{x}, t)$  and  $\bar{f}_{\alpha}(\mathbf{x}, t)$  denote the pre- and post-collision states of the distribution function, respectively.

As mentioned, the SRT collision model unfortunately suffers from severe disruptive numerical instabilities at relatively high Reynolds numbers, unless a high resolution lattice nodes is employed. It makes the SRT model to be computationally expensive for simulation of such flow conditions. Herein, the regularized lattice Boltzmann (RLB) scheme is employed to eliminate instabilities with suppressing the influence of higher order moments, which may oscillate rapidly. The

employed RLB collision model is based upon the idea that the hydrodynamic limits of the SRT model are not dependent on the details of the particle distributions, but only on the value of the first three moments, including density, velocity and stress tensor. These macroscopic variables can be defined through a multiscale Chapman-Enskog analysis of the LBM with BGK approximation which obeys the Navier-Stokes equations for weakly compressible flows. In this analysis, a power-law series with respect to a small parameter  $\varepsilon \ll 1$  is used to separate the physical phenomena happening at different scales as

$$f_{\alpha} = \sum_{k=0}^{\infty} \varepsilon^k f_{\alpha}^k \quad (10)$$

To asymptotically recover the dynamics of the N-S equations, the two first terms of order  $O(\varepsilon^0)$  and order  $O(\varepsilon^1)$  are sufficient (Latt and Chopard, 2006),

$$f_{\alpha} = f_{\alpha}^{(0)} + \varepsilon f_{\alpha}^{(1)} + O(\varepsilon^2) \quad (11)$$

The component  $f_{\alpha}^{(0)}$  of the particle populations is equal to the equilibrium distribution,  $f_{\alpha}^{(0)} = f_{\alpha}^{eq}(\rho, \mathbf{u})$ . The component  $f_{\alpha}^{(1)}$  reads

$$f_{\alpha}^{(1)} = -\frac{\omega_{\alpha}}{c_s^2} [Q_{\alpha} : \rho \nabla \mathbf{u} - \mathbf{e}_{\alpha} \nabla : \rho \mathbf{u} \mathbf{u} + \frac{1}{2c_s^2} (\mathbf{e}_{\alpha} \cdot \nabla)(Q_{\alpha} : \rho \mathbf{u} \mathbf{u})] \quad (12)$$

where contains a dominating term proportional to  $\mathbf{u}$  and two terms scaling as the square of  $\mathbf{u}$  which can be canceled in the RLB scheme for symmetry reasons (Latt *et al.* 2008). With this approach, the RLB model enhances stability by eliminating higher order, non-hydrodynamic terms from the particle populations. Recently, the stability and convergence properties of this collision model have been thoroughly studied by Montessori *et al.* (2014).

In the present paper, the RLB method is implemented with the approximation of the first-order multi-scale Chapman-Enskog expansion term as follows (Latt *et al.* 2008)

$$f_{\alpha}^{(1)} = \frac{\omega_{\alpha}}{2c_s^4} Q_{\alpha ij} : \Pi_{ij}^{non-eq} \quad (13)$$

where,  $Q_{\alpha ij} = e_{\alpha i} e_{\alpha j} - c_s^2 \delta_{ij}$  is a tensor and  $\Pi_{ij}^{non-eq} = -c_s^2 \tau (\partial_i \rho u_j + \partial_j \rho u_i)$  is the non-equilibrium momentum flux tensor. Then, the non-equilibrium distribution function  $f_{\alpha}^{non-eq} = f_{\alpha} - f_{\alpha}^{eq} \approx f_{\alpha}^{(1)}$  is used to approximate the collision operator in Eq. (2). Finally, the collision in Eq. (8) is applied to  $\bar{f}_{\alpha} = f_{\alpha}^{eq} + f_{\alpha}^{(1)}$ , which gives the regularized collision step as

$$f_{\alpha}(\mathbf{x} + \mathbf{e}_{\alpha} \Delta t, t + \Delta t) = f_{\alpha}^{eq}(\mathbf{x}, t) + (1 - \frac{1}{\tau}) f_{\alpha}^{(1)}(\mathbf{x}, t)$$

(14)

The regularization of the distribution function and executing the collision consecutively have the effect of a diagonalizable linear operation on the non-equilibrium part of the particle populations. Therefore, the relaxation parameters in the RLB scheme is determined from a physical argument based on the Chapman-Enskog expansion, not only on the numerical stability analysis.

Note that the regularized operation in this approach needs to implement at the boundaries similar to the flow field. Defining proper boundary conditions is then necessary in the RLB scheme for reconstruction of the unknown distribution functions at the domain boundaries. The following approach proposed by *Latt et al. (2008)* is used to model  $f_\alpha^{(1)}$  for implementation of the ‘‘regularized boundary condition’’:

First, all unknown distribution functions  $f_\alpha$  are assumed to obtain by a bounce-back of non-equilibrium parts, as

$$f_\alpha = f_\alpha^{eq} + f_{\alpha(opp)} - f_{\alpha(opp)}^{eq} \quad (15)$$

where  $f_{\alpha(opp)}$  and  $f_{\alpha(opp)}^{eq}$  are the known particle populations in the opposite lattice directions of the unknown ones. The distribution functions calculated by means of Eq. (15) are used to evaluate the value of  $\prod_{ij}^{non-eq}$  at the domain boundaries.

Then, Eq. (13) is employed to determine the  $f_\alpha^{(1)}$  and it therefore is used to construct all particle populations on the boundary nodes,

$$f_\alpha = f_\alpha^{eq} + f_\alpha^{(1)} \quad (16)$$

It should be noted that the macroscopic parameters  $\rho$  and  $\mathbf{u}$  are recovered appropriately by this boundary condition (*Latt et al. 2008*).

### 3. RESULTS AND DISCUSSIONS

This section contains the numerical results obtained for the dipole vorticity dynamics colliding a no-slip wall in a bounded flow by employing the RLB scheme implemented with different Reynolds numbers. An investigation is considered for studying the structure of separated boundary layer near the wall after interaction of the dipole vorticity. The results obtained by applying the present RLB method are compared with the available numerical results to demonstrate the accuracy of the computation technique applied.

#### 3.1 Problem Setup

The dipole vorticity dynamics is studied in a square bounded domain  $-1 \leq x, y \leq 1$  with the no-slip boundary conditions implemented on the all sides. To define two counter-rotating monopolar vortices, the velocity field is initialized as

$$u_0 = -\frac{1}{2}|\eta_e|(y - y_1)e^{-\left(\frac{r_1}{r_0}\right)^2} + \frac{1}{2}|\eta_e|(y - y_2)e^{-\left(\frac{r_2}{r_0}\right)^2}$$

$$v_0 = \frac{1}{2}|\eta_e|(x - x_1)e^{-\left(\frac{r_1}{r_0}\right)^2} - \frac{1}{2}|\eta_e|(x - x_2)e^{-\left(\frac{r_2}{r_0}\right)^2} \quad (17)$$

where  $(x_i, y_i)$  indicates the position of the positive and negative core vorticities by  $i = 1$  and  $2$ , respectively, and  $r_i = \sqrt{x_i^2 + y_i^2}$ . The parameter  $r_0$  is the core radius and  $\eta_e$  labels core vorticity. In the present work, the flow parameters are set as  $r_0 = 0.1$ ,  $\eta_e \approx 300$ ,  $(x_1, y_1) = (0, 0.1)$  and  $(x_2, y_2) = (0, -0.1)$ . Figure 1 shows the geometric parameters and initial dipole vortices in the middle of the computational domain that is indicated by the vorticity  $\Omega$  contours. In the all figures, the blue and red colors denote contours of negative and positive values, respectively,  $\Omega_{min} = 0.01$ ,  $\Omega_{max} = 0.2$  and  $\Delta\Omega = 0.01$ .

The computations are carried out for values of Reynolds numbers in the range of  $Re = 10^4 - 10^5$  and the results obtained for the unsteady flow structures and statistics are addressed. Note that the Reynolds number for this flow problem is defined as  $Re = U_{rms}N/\nu$ , where  $U_{rms}$  is the initial root mean square (rms) velocity and  $N$  is the number of lattice nodes along the half-side of square computational domain. Herein, the initial root mean square (rms) velocity is set to be  $U_{rms} \approx 0.001$  in lattice unit and consequently, the Mach number of the present solutions is of order  $M = U_{rms}/c_s \approx O(10^{-3})$ .

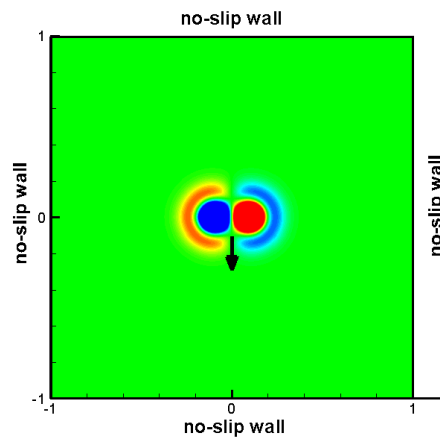
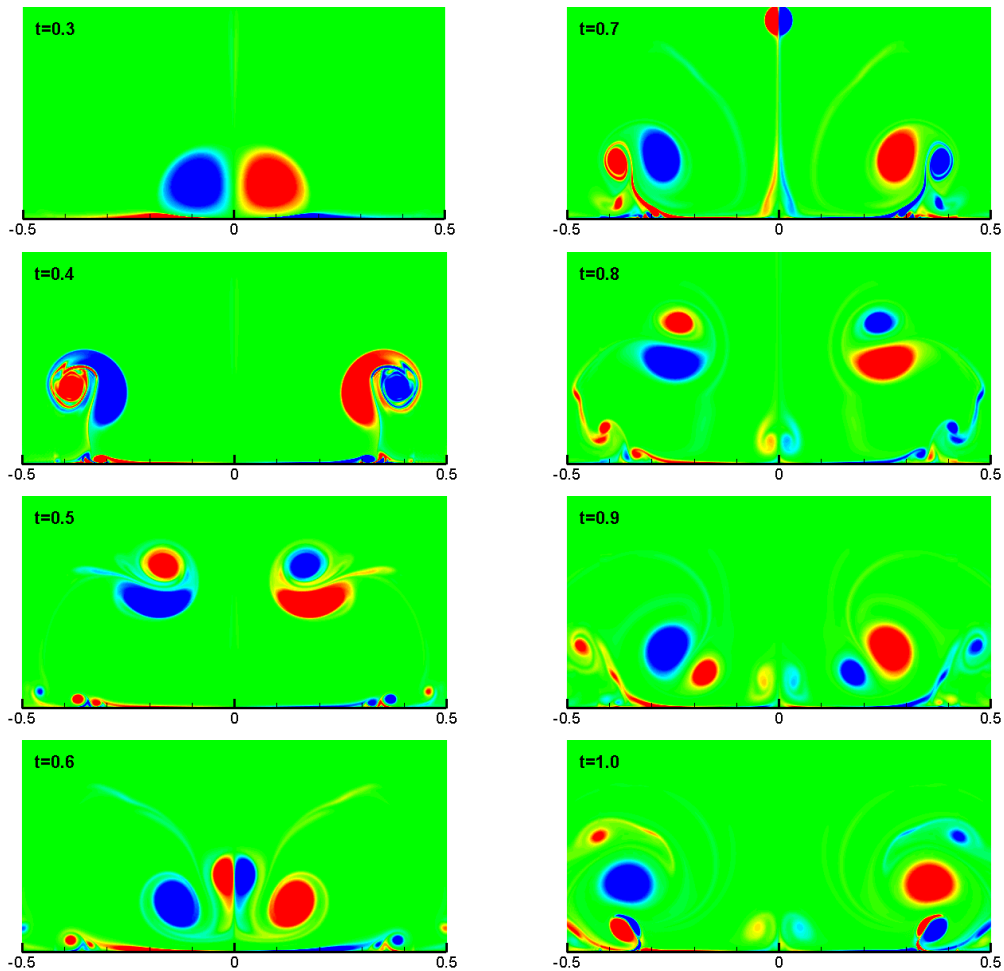


Fig. 1. Geometry and initial condition shown by vorticity field  $\Omega$  for studying the dipole vorticity dynamics colliding with the wall.

#### 3.2 Simulation of Dipole-Wall Collision

To obtain sufficiently accurate results and also to



**Fig. 2.** Sequence of computed flowfield near the bottom wall shown by vorticity contours for dipole vorticity dynamics colliding with no-slip wall at  $Re = 10^4$ .

**Table 1** Comparison of the results obtained for primary vortex position of dipole vorticity dynamics colliding with no-slip wall at  $Re = 10^4$

		Kramer <i>et al.</i> (2007)		Present Solution	
$t$	$x_{mv}$	$y_{mv}$	grid size	$x_{mv}$	$y_{mv}$
0.6	0.2562	0.0961	(200×200)	0.2913	0.1184
			(400×400)	0.2724	0.0940
			(800×800)	0.2708	0.0937
1.0	0.6439	0.2738	(200×200)	0.7921	0.2985
			(400×400)	0.6582	0.2719
			(800×800)	0.6518	0.2701

have stable numerical solutions at high Reynolds numbers, a special effort on grid resolution is required. In the present work, 400 lattice points are used along the side wall of the square flow domain for  $Re = 10^4$  (see Table 1). Subsequently, the grid resolution for higher Reynolds numbers  $Re = 2 \times 10^4$ ,  $5 \times 10^4$  and  $10^5$  are increased by 800, 1200 and 1600 grid points, respectively.

Figure 2 shows the instantaneous vorticity field  $\Omega$  for the dipole colliding the no-slip wall at

$Re = 10^4$ . As seen in this figure, the dipole vortices separate after colliding and move along the no-slip wall in opposite directions at the dimensionless times  $t = 0.3, 0.4$ . The flow advection and detachment from the wall are obvious at  $t = 0.4$ . Consequently, two secondary asymmetric dipole vortices are formed and lead to secondary collision with the no-slip wall at  $t = 0.5, 0.6$ . It is observed that another small scale dipole is formed at the center line of the flow domain at  $x = 0$  which translates away from the wall along the

$y$  – direction (see  $t = 0.7$ ). After secondary dipole vortices roll up and collide with the wall, even more flow detaches from the boundary layer at  $t = 0.8 - 1.0$  which leads to formation of multiple small vortices. It should be noted that the flow field is left-right symmetry, but top-bottom asymmetry. A sequence of vorticity contour plots in Fig. 3 shows the production of vorticity patches near the top wall due to colliding of small scale dipole formed at the center line of the flow domain. These dipole vortices collide the top wall and form another small scale dipole vorticity dynamics near the top wall which its structure is different than that of formed near the bottom wall.

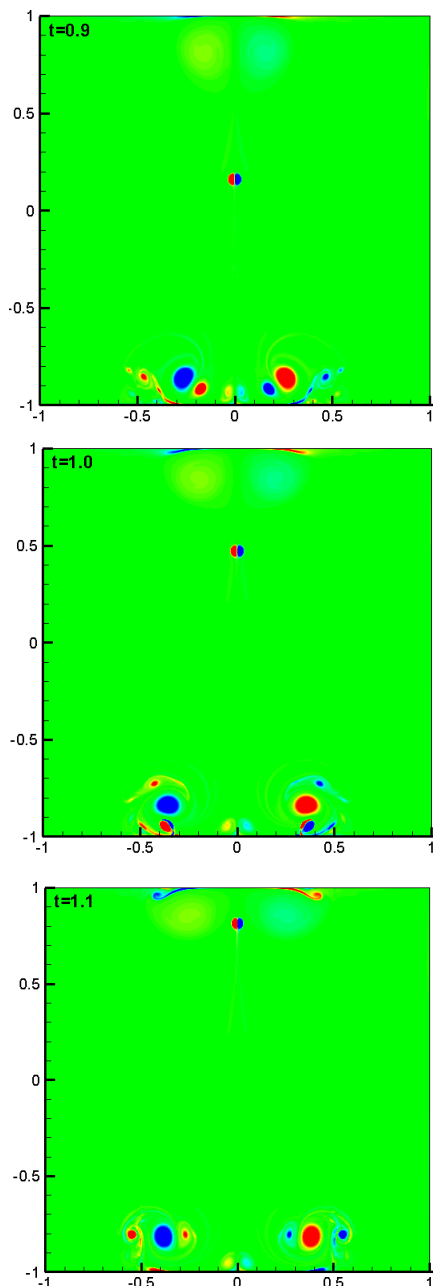


**Fig. 3. Sequence of computed top-bottom asymmetry flowfield shown by vorticity contours for dipole vorticity dynamics colliding with no-slip wall at  $Re = 10^4$ .**

To verify the accuracy of the present numerical simulations based on the RLB scheme, the results obtained for position of the maximum vorticity in the dipole-wall colliding flow domain at  $Re = 10^4$  are compared to the available benchmark results reported by *Kramer et al. (2007)*. In Table 1 the locations of the maximum vorticity in the flow field,  $(x_{mv}, y_{mv})$ , are given for the positive half of the dipole. Note that the location is measured relative to the point where the central axis of the dipole crosses the bottom no-slip wall. A grid refinement study is conducted to present the mesh convergence of the primary vortex position for the dipole vorticity dynamics colliding with no-slip wall at  $Re = 10^4$ . The computational grids used for the study of mesh convergence are uniform throughout with  $(200 \times 200)$ ,  $(400 \times 400)$  and  $(800 \times 800)$  lattice points. It is shown that the grid  $(400 \times 400)$  is appropriate for an accurate solution of this problem at the given flow condition by implementing the RLB scheme employed and further grid refinement does not significantly improve the accuracy of the results. As seen in this table, there is a good agreement for the positions obtained by the present numerical scheme based on the RLB method in comparison with those of reported in literature based on the N-S flow solver which confirms the accuracy of the present simulations. It should be noted that a second order polynomial is used by *Kramer et al (2007)*. to fit the vorticity field for determining the positions. However, the data reported in the present work are based on the grid resolutions used which may cause a slight difference between the results reported in Table 1.

The flow pattern of the dipole colliding with the wall is more interesting for higher Reynolds numbers. Figure 4 demonstrates the time evaluations of the dipole dynamics after first collision with the no-slip wall at  $Re = 2 \times 10^4$ ,  $5 \times 10^4$  and  $10^5$ . Since this flow problem has a left-right symmetry pattern, the vorticity contours are presented for the right part of the domain for the sake of summarizing. In these cases, the flow separation near the boundary layer at  $t = 0.4$  and its movement along the wall after the first dipole collision are obviously similar to the flow pattern observed for  $Re = 10^4$ . However, the differences between these cases are visible after rolling up of the secondary dipole vortices for the next encounter with the wall. The flow fields presented at  $t = 0.6$  and  $0.8$  show that the vorticity filaments near the wall are thinner but stronger in amplitude for higher Reynolds numbers. Due to the higher vorticity amplitude of induced boundary-layer for higher Reynolds numbers, some vortices detached from the wall around the secondary vortex are advected in form of multiple small vortices. In Fig. 4, this phenomenon can be observed after  $t = 0.8$  for the considered cases, which is different from the detached mechanism of the secondary vortices captured for  $Re = 10^4$ . The present numerical

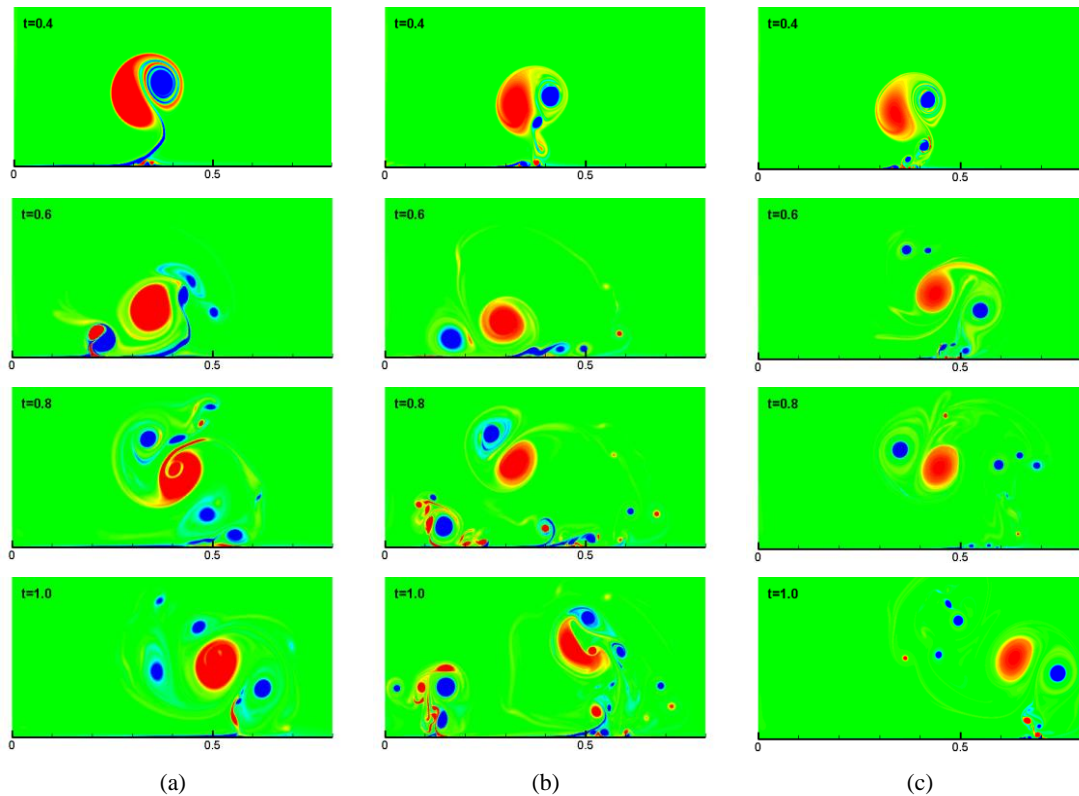


**Fig. 4. Sequence of computed flowfield shown by vorticity contours for dipole vorticity dynamics colliding with no-slip wall at (a)  $Re = 2 \times 10^4$ , (b)  $Re = 5 \times 10^4$ , and (c)  $Re = 10^5$ .**

results obtained based on the RLB scheme shows that the primary and secondary vortices have almost similar structures for  $Re = 5 \times 10^4$  and  $10^5$ . However, for  $Re = 10^5$ , the small-scale vortices formed near the wall and also around the symmetry line of the flow domain reach a very high vorticity, which create very chaotic and strong vortices. This phenomenon of symmetry breaking of dipole vorticity and then spontaneous spin-up due to interaction with no-slip wall at very high Reynolds numbers turns out to be crucial for the production of angular momentum. Keetels *et al.* (2010) have thoroughly studied this phenomenon as a decaying turbulent flow in square containers.

Figure 5 shows the vorticity  $\Omega$  distribution on the bottom wall after the dipole collision at  $t = 0.4$  for three Reynolds numbers  $Re = 2 \times 10^4$ ,  $5 \times 10^4$  and  $10^5$ . In this figure, the vortex and boundary layer vorticity visualized by the light gray contours which the solid and dashed lines indicate positive and negative values, respectively. As seen in Fig. 5, the vorticity changes sign ( $\Omega|_{y=0}$ ) in some points on the wall. These points are dynamically very important to define the start and end positions of the streamlines which indicate the flow separates from, or attaches to the wall, respectively. Therefore, the small regions between the two points with  $\Omega|_{y=0}$  indicate the presence of recirculation in the boundary layer. From the intense picks in these

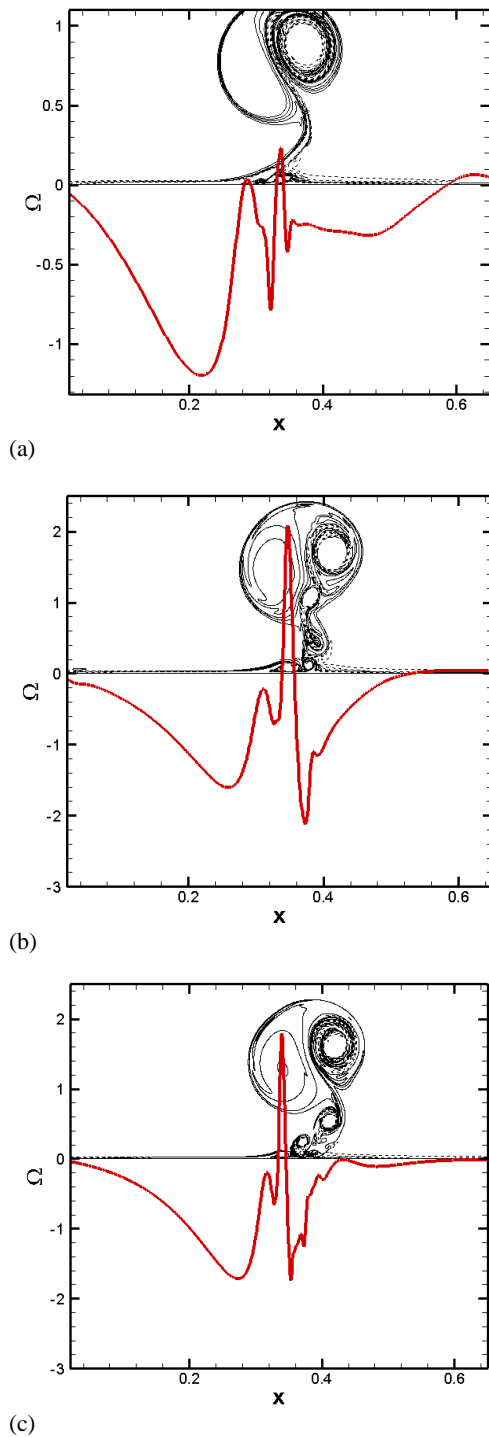
plots for higher Reynolds numbers, it can be inferred that strong shear-layer instabilities near the wall at higher Reynolds numbers lead to intensive eruptions of boundary-generated vorticity which cause the roll-up and formation of a number of small-scale vortices.

The dipole collision with the no-slip wall studied in the present work is characterized by a 2-D turbulent dynamics where the wall acts as a source of small scale vortices originated from the detached boundary-layer. To quantify the decay rate of the total energy in this bounded viscous flow field, the average enstrophy  $\langle \Phi \rangle$  is computed based on the squared vorticity in the domain:

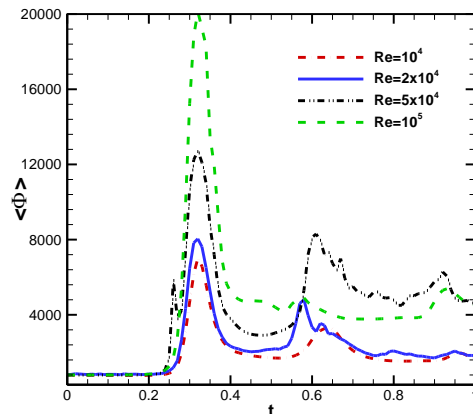
$$\langle \Phi \rangle = \frac{1}{2} \int_{-1}^1 \int_{-1}^1 \Omega^2(x, y) dx dy \quad (18)$$

Figure 6 indicates the instantaneous average enstrophy  $\langle \Phi \rangle$  evaluated for the flow conditions considered. This figure shows distinct peaks of  $\langle \Phi \rangle$  for the all Reynolds numbers studied which coincide with the first and second collisions of the dipole with the wall. It can be concluded that the boundary-layer near the wall builds-up a large amount of vorticity at the moment of dipole-wall collision which has the main contribution to the average enstrophy (Kramer *et al.*, 2007). Note that the maximum value of the average enstrophy increases with increment of the Reynolds number

due to the strong amplitude of the vorticity filaments near the wall at such flow condition. Some smaller peaks in the enstrophy curve of the dipole-wall collision with  $Re = 5 \times 10^4$  and  $10^5$  indicate rebounds of the small-scale vortices generated in the boundary layer at such flow conditions.



**Fig. 5. Vorticity distribution on the bottom wall after dipole collision at  $t = 0.4$  for (a)  $Re = 2 \times 10^4$ , (b)  $Re = 5 \times 10^4$ , and (c)  $Re = 10^5$ .**



**Fig. 6. Comparison of instantaneous averaged enstrophy in the flow domain for dipole vorticity dynamics colliding with no-slip wall.**

#### 4. CONCLUSIONS

In the present work, the dipole-wall collision is considered as a model problem to investigate vortex interactions with the wall at high Reynolds numbers. The lattice Boltzmann method with the regularized collision model is implemented for studying the separated fluid flow characteristics and statistics. It is demonstrated that the shear instability occurred in the boundary layer at high Reynolds numbers makes strong vorticity eruptions in the secondary vortices formed and creates multiple small-scale vortices between the dipole half and the no-slip boundary. The time evaluation of the average enstrophy for this problem confirms that although the vortices injected into the flow after collision become smaller for higher Reynolds number, but they have a higher vorticity amplitude. Also, the results computed based on the present RLB scheme show that the simulations account well the flow characteristics and essential features of the separating shear-layers at high Reynolds numbers with stable numerical solutions. Development of the present numerical approach as a DNS solver in 3-D framework will be considered in the future work for simulation of three-dimensional turbulent flows.

#### ACKNOWLEDGEMENTS

The author would like to thank Shahid Beheshti University for the support of this research.

#### REFERENCES

Clercx, H. J. and C. H. Bruneau (2006). The normal and oblique collision of a dipole with a no-slip boundary. *Computers & Fluids* 35, 245-279.

Clercx, H. J. and G. J. van Heijst (2002). Dissipation of kinetic energy in two-dimensional bounded flows. *Physical Review E* 65, 066305.

Coutsias, E. A. and J. P. Lynov (1991). Fundamental interactions of vortical structures with boundary layers in two-dimensional flows. *Physica D: Nonlinear Phenomena* 51,

- 482-497.
- Du, R., B. Shi and X. Chen (2006). Multi-relaxation-time lattice Boltzmann model for incompressible flow. *Physics Letters A* 359, 564–572.
- Ezzatneshan, E. (2018), Comparative Study of the Lattice Boltzmann Collision Models for Simulation of Incompressible Fluid Flows. *Mathematics and Computers in Simulation* 156, 158-177.
- Karlin, I. V., A. N. Gorban, S. Succi and V. Boffi (1998). Maximum entropy principle for lattice kinetic equations. *Physical Review Letter* 81, 6–9.
- Keetels, G. H., H. J. H. Clercx and G. J. F. van Heijst (2010). On the origin of spin-up processes in decaying two-dimensional turbulence. *European Journal of Mechanics* 29, 1–8.
- Kramer, W., H. J. Clercx and G. J. F. van Heijst (2007). Vorticity dynamics of a dipole colliding with a no-slip wall. *Physics of Fluids* 19, 126603.
- Lagrava, D., O. Malaspinas, J. Latt and B. Chopard (2012). Advances in multi-domain lattice Boltzmann grid refinement. *Journal of Computational Physics* 231, 4808-4822.
- Latt, J. and B. Chopard (2006). Lattice Boltzmann method with regularized non-equilibrium distribution functions. *Mathematics and Computer in Simulation* 72, 165–168.
- Latt, J., B. Chopard, O. Malaspinas, M. Deville and A. Michler (2008). Straight velocity boundaries in the lattice Boltzmann method. *Physical Review E* 77, 056703.
- Luo, L.-S., W. Liao, X. Chen, Y. Peng and W. Zhang (2011). Numerics of the lattice Boltzmann method: Effects of collision models on the lattice Boltzmann simulations. *Physical Review E* 83, 056710.
- Montessori, A., G. Falcucci, P. Prestininzi, M. L. Rocca and S. Succi (2014). Regularized lattice Bhatnagar-Gross-Krook model for two-and three-dimensional cavity flow simulations. *Physical Review E* 89 (5), 053317.
- Orlandi, P. (1990). Vortex dipole rebound from a wall. *Physics of Fluids A: Fluid Dynamics* 2, 1429-1436.
- Wells, J. and Y. D. Afanasyev (2004). Decaying quasi-two-dimensional turbulence in a rectangular container: Laboratory experiments. *Geophysical & Astrophysical Fluid Dynamics* 98, 1-20.
- Wells, M. G., H. J. H. Clercx and G. J. F. van Heijst (2007). Vortices in oscillating spin-up. *Journal of Fluid Mechanics* 573, 339-369.